

# Determination of human EEG alpha entrainment ERD/ERS using the continuous complex wavelet transform

David B. Chorlian<sup>\*a</sup>, Bernice Porjesz<sup>a</sup>, Henri Begleiter<sup>a</sup>

<sup>a</sup>Neurodynamics Laboratory, SUNY/HSCB, Brooklyn, NY, 11203

## Abstract

Alpha entrainment caused by exposure to a background stimulus continuously flickering at a rate of 8 1/3 Hz was affected by the appearance of a foreground target stimulus to which the subjects were requested to press a button. With the use of bipolar derivations (to reduce volume conduction effects), scalp recorded EEG potentials were subjected to a continuous wavelet transform using complex Morlet wavelets at a range of scales. Complex Morlet wavelets were used to efficiently calculate instantaneous amplitudes and phases on a per-trial basis. Multiple scales were employed to contrast the pattern of alpha activity with those in other bands, and to determine whether the harmonics observed in the spectral analysis of the data were simply a result of the non-sinusoidal response to the entraining signal or a distinct neural phenomenon. We were thus able to calculate desynchronization/resynchronization for both the entrained and non-entrained alpha activity. The occurrence of the target stimulus caused a sharp increase in amplitude in both the entrained and non-entrained alpha activity, followed by a sharp decrease, and then a return to baseline, over a period of 2.5 seconds. However, the entrained alpha activity showed a much more rapid recovery than non-entrained activity.

**Keywords:** EEG, wavelet, Morlet, desynchronization, entrainment

## 1. Introduction

The aim of this paper is neither mathematical nor neurophysiological, but rather to show how some well known mathematical methods can be applied to neurophysiological data in order to illuminate some recent discussions on the role of ongoing oscillatory processes in evoked potential activity<sup>1</sup>. The application of the continuous complex wavelet transform to single trial data enables both phase and amplitude information to be extracted and then compared across trials to determine whether amplitude or frequency modulation has occurred in bands of interest. In our case, we are interested in the effect of an oddball task superimposed on entrainment, but the methods developed here can be used on a variety of other types of experiments.

## 2. Description of Experiment

The object of the experiment is to produce the entrainment of alpha EEG activity by photic driving, and to affect the entrainment by imposing an oddball task. Entrainment occurs when some aspect of brain activity becomes synchronized with a periodic stimulus. The oddball task requires the subject to press a button whenever an infrequently occurring foreground stimulus appears. Entrainment is induced through the use of a flashing background stimulus on which a non-flashing foreground stimulus appears. The background stimulus is a square on the video screen that is white for 60 milliseconds and then black for 60 milliseconds continuously throughout the approximately 12 minutes of the experiment; this produces an 8 1/3 Hz. photic driving. The foreground stimulus is either the letter 'A' or the numeral '5', presented in red. The experiment is divided into trials, 3.25 seconds in length, such that the background stimulus is the same at each sample across trials. In each trial, either the 'A' or the '5' appears on the screen for the duration of the trial. The '5' occurs in 13% of the trials in a pseudo-random sequence, and the subject is directed to push a button when it appears on the screen. Thus the foreground stimulus changes only on the appearance of the target stimulus in place of the non-target stimulus, and the replacement of the target stimulus by the non-target stimulus 3.25 seconds later. The interval between successive target trials ranges from 6.5 to 30 seconds. An examination of the averaged signal in which the trials are grouped into target, non-target, and non-target after target reveals considerable entrainment, with distinct peaks in the power spectrum at 8 1/3 and 16 2/3 Hz.

---

\* chorlian@cns.hscbklyn.edu

### 3. Method of Analysis

The segmentation of EEG recordings into short time periods is essentially arbitrary, as there are no stimuli or other events to dictate the segment boundaries. Thus comparisons across segments are independent of the actual time involved. In evoked potential records, stimulus presentation or other significant events, such as subject response, form natural boundaries for segmentation. In these cases, meaningful cross-trial time related comparisons are possible. However, since the boundaries are either aperiodic or have a period far longer than that of typical human brain activity, oscillatory brain activity is not generally synchronized with these events. Thus most cross-trial analyses have been simply devoted to aggregating single trial results. An important exception is the paper by Makeig et.al. (2002)<sup>2</sup>. That paper attempts to demonstrate that the appearance of a stimulus induces a frequency modulation in alpha activity which causes a cross-trial synchronization in a period about 200 ms. after stimulus presentation. In our experimental situation, the presence of the 8 1/3 Hz. background stimulus forces some oscillatory activity, at least in the alpha band, to be synchronized with the foreground stimulus presentation. While this complicates the experimental design, it enables powerful mathematical methods to be applied to cross-trial data on a sample by sample basis.

In order to determine the precise temporal course of oscillatory activity, an analytic method which is capable of a high degree of temporal resolution is required, as well as a moderate width in the frequency domain. Power spectral methods, whether based on the Fourier Transform or an auto-regressive procedure, suffer from the fact that a fixed size time window is used for all frequency estimations, which leads to significant loss of time resolution for the higher frequency components. On the other hand, the precise frequency resolution of power spectral methods does not offer a counterbalancing advantage, since we expect the activity in different frequency bands to exhibit some degree of amplitude and frequency modulation. In order to meet these demands, a wavelet based method was used. The discrete wavelet transform, using scales of powers of 2 and non-overlapping time windows for each scale, suffers from coarse frequency resolution and translation non-invariance (choice of a starting time greatly affects results). The continuous wavelet transform method provides continuous output and the option of having multiple scales per octave<sup>3</sup>. This produces many more values than are needed for the reconstruction of the original signal, but yields results more suitable for visual interpretation. The complex Morlet wavelet was chosen for use because its sinusoidal shape approximates the shapes in the signal quite well. The use of a complex wavelet also enables phase relations to be examined directly. After visual inspection of the results, appropriate scales and time windows can be selected for statistical analysis. We must realize that our continuous results are not instantaneous results, but derive from an aggregating process which extends over a not-insignificant time range relative to the length of the features in the signal itself. The presence of some seemingly anti-causal effects, as a rise in a low-frequency amplitude before the event which purportedly causes the rise, simply reflects the fact that in the presentation of the data, the aggregating time range extends both into the future and past of the point at which the value is presented.

The data were collected at a sampling rate of 256 samples per second from a 61 electrode montage in 42 control subjects. Blinks were automatically removed offline by a spatial filtering method, and uncorrectable trials were removed from further analyses. The data were transformed to bipolar form by subtracting signals from adjacent electrodes to produce 52 channels oriented vertically. Bipolar derivations were used to reduce volume conduction effects, and thus effect some degree of source localization<sup>4</sup>. The vertical orientation seemed to reveal a more interesting pattern of data than the horizontal, so we focused on it. For purposes of averaging, trials are grouped by their time from the target stimulus and ordered so that we have a 1.6 second pre-target-stimulus interval followed by a 9.75 post-target-stimulus interval in the data subject to analysis. The post-target-stimulus interval includes the reappearance of the non-target foreground stimulus. The data were resampled in order to have an integral number of sample points per 120 ms. cycle of background stimulus presentation. That is, every 32nd point in the resampled data corresponds to exactly the same stage of background stimulus presentation. The resampling enabled the choice of scales for the wavelet transform to exactly match the period of the entraining stimuli and its harmonics. For the sake of completeness, the octave separated scales were supplemented with three additional scales for each octave, and placed as evenly as possible given the constraint of integer values for the scales. The scales ranged from 9 to 128, providing a range of from about 56 Hz to 4 Hz for the center frequencies of the Morlet wavelets. The complex wavelet transform is a convolution of the input signal with an appropriately scaled complex sinusoid

within an  $e^{-x^2}$  window.

$$u(t, a) = \sum_{-\tau}^{\tau} (s(t + \tau) * w(t, a))$$

where  $\tau = a/2$ , with  $a$  the scaling factor, and

$$w(t, a) = 1/\sqrt{a} \exp(-(t/a)^2/2) * \exp(2\pi i(t/a))$$

The convolution of the complex Morlet wavelet with the data results in an array of complex-valued time series for each subject. To produce the time-series of non-time-locked values, the amplitude of the element of the complex array is calculated, and then averaged across trials. To produce the time-series of time-locked values, the complex values are averaged across trials and their amplitude is then calculated. Simply put, we find the average of the amplitudes and the amplitude of the average, each across trials, for every time, channel, and electrode scale. The relation between these two time series of amplitudes of wavelet transformed data will form the basis of our analysis. If we assume that our data is produced by a single source, the mean amplitude of the source in a scale is the mean across trials of the amplitude of the time series, which is given by the non-time-locked values. The degree of the entrainment is the ratio of the amplitude of the wavelet transform of the data averaged across trials, the time-locked values, to the mean amplitude, since signals consistently aligned with the stimuli will be aligned across trials, while non-entrained components will be randomly aligned with the stimuli, and through vector addition cancel out. However, this is an inexact measure, because we cannot expect entrained activity to be exactly similar in each trial. The time series of the ratio of the time-locked to non-time-locked values measures the consistency of phase and correlation of amplitude with phase of the source across trials, and will be called the intertrial coherence (ITC),

$$\left| \frac{\sum u_i}{\sum |u_i|} \right| = ITC$$

by analogy with the spectral measure of coherence. Since consistency in phase across trials is consistency in phase with regard to the entraining stimuli, this is our best metric of the degree of entrainment of the signal. If we suppose that the single source activity is superimposed on some small random non-entrained activity, the ITC is further diminished in our case because we cannot expect the sum of the non-entrained activity to cancel out by addition over the trials, as we do not have enough trials to ensure this.

However, as we shall see when we examine the wavelet transformed results, a single source is unlikely. Rather, there seem to be two distinct sources, one entrained to the background stimulus, the other not. The non-entrained activity does not appear to have a random phase distribution, or one that is the same at all times. In the two source model, the interpretation of the time-locked and non-time-locked amplitudes is considerably more complicated. The time-locked amplitude is roughly the sum of the entrained amplitude and the non-entrained amplitude multiplied by its ITC but diminished to the degree that mean phase of the non-entrained activity differs from the phase of the entrained activity. The non-time-locked amplitude is always less than the sum of the mean amplitudes of the activities, the amount depending upon the phase relations of the entrained and non-entrained activity. Thus in this case the ITC is not the measure of consistency in phase of a single source across trials, but measures both the consistency in phase of both sources as well as the relation of the amplitude of the entrained to the non-entrained activity. Unfortunately, a quantitative model of these relations is dependent upon arbitrary assumptions about distributions in phase and amplitude of the underlying sources. (The appendix contains a more comprehensive discussion of this topic.) It would therefore be premature to derive quantitative measures of entrained and non-entrained activity from the wavelet transformed results. However, we will speculate about these relations by drawing on topographic and temporal information. In particular, we will attempt to characterize intervals of increase and decrease of ITC both in terms of changes in amplitude of the entrained activity and of the phase resetting (frequency modulation) of non-entrained activity. Phase resetting occurs when the occurrence of a stimulus advances or retards activity so as to produce a more concentrated phase distribution at some subsequent time.

We can use a similar metric the consistency of phase between signals at two different frequencies. We will call this interfrequency phase coherence.

$$\left| \frac{\sum u_i v_j}{\sum |u_i v_j|} \right| = IPC$$

Examination of the time series of interfrequency phase coherence will shed light on the question of whether the peak at the first harmonic of the driving frequency we observe in the power spectrum of the data is the result of the periodic but non-sinusoidal shape of the response to the entraining stimulus, or represents the activity of a separate neural process. If the peak in the power spectrum were purely the result of the periodic but non-sinusoidal shape of the response to the entraining stimulus, the phase of the wavelet transform centered on the first harmonic at any time would depend completely on the phase of the wavelet transform centered on the driving frequency at that time. The measured phase consistency of the two signals or rather their wavelet transforms would be the same as the phase consistency of the driving frequency alone.

## 4. Results

### 4.1 Data Presentation

In order to see the temporal and topographic results of our analysis, the values from the wavelet transform are presented visually in a variety of ways. The first three figures have contour plots using all the scales and averaging over all the channels. The values are presented as derived, and as a Z score for each scale considered separately. The Z score presentation allows the temporal structure of each scale's values to emerge, rather than being obscured by overall amplitude differences. The time scale extends from 500 milliseconds preceding the appearance of the target stimulus to 4500 milliseconds subsequent to the stimulus. The change of the foreground stimulus from the target to the non-target occurs 3250 milliseconds subsequent to the stimulus. The frequency scale is logarithmic and extends from about 4 Hz to about 50 Hz. Horizontal lines indicate the driving frequency and its first two harmonics. Colorbars indicate the correspondence of values with colors. Figures 4 through 7 show topographic maps on a considerably shorter time scale. Again, both directly derived amplitudes and their Z scores are presented.

We refer in the succeeding discussion to the theta, alpha, and beta frequency bands, traditionally given as 4-7 Hz, 8-12 Hz, and 13-28 Hz. The divisions found in our data are in rough correspondence with these bands, so we feel free to use that terminology without further qualification.

### 4.2 Global Results

The non-time-locked amplitude values clearly divide into three frequency regions characterized by initial activation period and intensity, succeeding deactivation period, and post-deactivation activity, without further topographic consideration (Figs 1-3). (Current terminology uses “synchronization” and “desynchronization” for activation and deactivation. But this use of “synchronization” does not relate to time relations of observable data, but to an underlying mechanism. We prefer to use terms that describe the data directly.) We note that the characterization is made more visible by presenting the Z score of each frequency scale; the untransformed amplitude values are dominated by the difference between frequency bands, which makes it difficult to see the varying temporal structure in each scale. The theta band activity, below about 6 Hz, is distinguished by the intensity of the initial activation, its persistence up to 700 ms. post-stimulus, and the duration of the deactivation period, extending to at least 2000 ms post-stimulus, considerably longer than that of the other bands. The alpha band activity, between about 6 Hz. and 13 Hz. has post-stimulus activation persisting to 350 ms. post-stimulus, deactivation to about 1500 ms. post-stimulus, followed by recovery. The increase of activity at about 3000 ms. post-stimulus could be some anticipatory activity in advance of the change of the foreground stimulus from the target to the non-target. Since there are 30 trials with this pattern, it is certainly possible that some unconscious learning is taking place. The beta band activity, above 13 Hz., is characterized by a much shorter deactivation period, and an intense activation from about 1000 ms to 1700 ms. post-target. It is unlikely that the post-target increase in beta range activity is related to the button push to the target, as it shows a similar increase after the appearance of the non-target stimulus. The patterns are replicated, but without the same intensity, in response to the change in the foreground stimulus from target to non-target.

The patterns noted above are much less distinctive in the time-locked values. This is because for most of the period, except for phase-resetting to the changes in the foreground stimulus, there is no real time-locking in the lower frequency activity, as can be seen from the global ITC values. The pronounced patterning above 13 Hz. probably reflects amplitude modulation induced by the entraining stimulus. In addition there is a pronounced difference in the frequency distribution of the time-locked values compared to the non-time-locked values. This is particularly notable in the alpha range, where the peak of the non-time-locked values is above the entraining frequency. This suggests that there are two distinct sources of alpha activity, one entrained and the other not.

#### **4.2 Topographic Results**

We turn our attention first to the 8 1/3 Hz. activity (Figs. 4, 6). The immediate post-stimulus increase of both time-locked and non-time-locked activity involves primarily a phase-resetting of the non-entrained activity engendered by the occurrence of the target stimulus. This can be concluded from the fact that the increase in the time-locked activity occurs at the foci of the non-time-locked activity; when the time-locked activity recovers following its recession from the immediate post-stimulus peak, the recovery has only a single occipital focus, centrally located. Again, there is a significant frontal increase in the immediate post-stimulus response, which is not present in the recovery phase. This is confirmed when we look at the Z scores of the ITC (Fig 6). In these, all activity from 4 Hz to approximately 16 Hz shows an immediate post-stimulus increase in ITC, with the driving frequency showing the least increase. This is because the presence of the entrained activity makes for a increased baseline ITC at the driving frequency. In terms of the topography of the ITC, we note that immediate post-stimulus increase is greatest frontally, with no significant increase occipitally. This seems to show that there is little phase resetting at the occipital focus of the entrained activity; it is probably as consistent across trials as possible. At the post-stimulus low, the occipital ITC is at its lowest. This cannot simply be the result of the "unlocking" of the non-entrained activity; the amplitude of the entrained activity must be declining more rapidly than the amplitude of the non-entrained activity. When the time-locked activity begins its increase after its post-stimulus low, the ITC increases most in the occipital and central regions. This reflects an increase in the entrained activity relative to the non-entrained activity. Thus we conclude that in the immediate post-stimulus (0-250 ms) period, both the amplitude of the entrained and non-entrained activity increases, as does the phase resetting of the non-entrained activity. In the succeeding period of decrease, both sources decrease, the entrained more rapidly than the non-entrained, but the entrained recovers its baseline level of amplitude more rapidly than does the non-entrained.

The two source model is further confirmed by the examination of the results of performing a singular value decomposition on the concatenation of the time-locked and non-time-locked values, and separating the temporal components belonging to the common spatial components (Fig 8). While the first component reveals what is common to the two sources, the second shows that the difference is the central occipital focus which is what we observed in comparing the topographies of the time-locked and non-time-locked values.

When we turn our attention to the beta range activity centered at the first harmonic (Figs 5, 6), we notice that the topography of the time-locked activity is quite similar to the activity at the driving frequency. However, the temporal patterns are almost the reverse of each other. While the alpha activity has an immediate post-stimulus increase followed by a decrease, the beta activity declines occipitally and then increases in the same periods. The non-time-locked values show a quite different topography than the time-locked values. This suggests again that there are two distinct sources: the entrained a response of the visual system, and the non-entrained something different. It would be tempting to attribute the non-central occipital foci to a harmonic of the 8 1/3 Hz non-entrained activity, but the interfrequency coherence topography does not support this (Fig 7). The interfrequency coherence values suggest that the increase in ITC during the 750-1000 ms. period is the result of an increase in entrained activity, possibly linked to the increase of entrained activity at the driving frequency. The variability of the interfrequency coherence values support the temporal values in establishing that the entrained beta activity is not simply a harmonic of the entrained alpha activity.

Clearly there are a variety of conclusions which can be drawn by using these methods. Further directions of study would include a comparison of the response to the non-target stimulus to the response to the target stimulus, and a comparison with the data from the same subjects on an oddball task without entrainment.

## Appendix

We calculate the amplitude of the activity in any frequency band both on a per-trial basis and on the average across trials. The ratio between the activity calculated from the average across trials and that calculated on a per-trial basis measures the phase consistency of activity across trials. If the activity were completely and perfectly entrained, the ITC would have a value of 1. If this ITC is very small at a site, then we can conclude that there is no entrainment occurring, since with the relatively small number of trials being averaged, the likelihood is that the average across trials will not be zero. On the other hand, if the ITC is above a certain value (about .2, based on the number of trials included in our average for each subject)<sup>5</sup>, then we can safely conclude that there is some entrained activity at the site. Let us take as our first model of the system the sum of entrained activity with constant amplitude and variable ITC, and non-entrained activity with constant amplitude and phases which have a uniform distribution over the range  $-\pi$  to  $\pi$ . Then the mean amplitude of the entrained activity is close to the time-locked-value. Because of the varying phase relations across trials between the entrained and non-entrained activity, we cannot interpret the ITC of the overall activity as the ratio between the amplitude of the entrained activity and the sum of the amplitudes of the entrained and non-entrained activity. Instead we can draw the following conclusions: For a constant value of the relative amplitudes of the entrained and non-entrained activity, the greater the ITC of the entrained activity, then the greater the ITC of the overall activity. Similarly, for a constant value of the ITC of the entrained activity, the greater the relative amplitude of the entrained activity the greater the ITC of the overall activity. Thus, for any degree of overall ITC there are two controlling factors, the relative amplitude of the entrained activity to the non-entrained activity and the degree of ITC of the entrained activity, which are inversely related. The variance of the amplitude across trials is a function of the relative amplitudes of the entrained activity and the non-entrained activity, and not of the ITC of the entrained activity. (This is because if the non-entrained activity has random phase, the sum of the non-entrained activity and the entrained activity is a function only of the amplitudes of the activities and the angle between them. If the angles of one vector have a uniform distribution, the angles of the difference between the two vectors will have a uniform distribution so long as the angles of the second vector are uncorrelated with the first.) The variance of the amplitude across trials will be lowest at the extremes of the ratios of amplitudes, and higher when they are more nearly equal. Thus for a given variance of amplitudes across trials, we may find that there are two ratios of amplitudes possible. But we also know that the observed value of the overall ITC must be greater than the ratio of amplitudes of the entrained and non-entrained activities. So if we observe an increase in the ITC of the overall activity, and the variance of amplitudes decreases, then the amplitude of the entrained activity increases. If the variance of the amplitude is unchanged or increases, then the ITC of the entrained activity increases. These relations will hold if we add variable ITC to the non-entrained activity to model phase resetting. Space precludes describing the precise quantitative relations involved.

## Acknowledgements

I wish to thank the many members of the staff of the Neurodynamics Laboratory for their help with this project. I had numerous productive discussions with Kongming Wang about the mathematical aspects of the analysis, and Kevin Jones and Keewhan Choi helped me clarify my arguments. Madhavi Rangaswamy helped to ensure that the conclusions that I drew from the results of the analysis were not utterly absurd.

## References

1. S. Makeig, et. al., *Dynamic Brain Sources of Visual Evoked Responses*, Science, Vol. 295, pp 690-694, 2002. See the references in that paper for further details.
2. See previous note.
3. S. Mallat, *A Wavelet Tour of Signal Processing*, Academic Press, San Diego, 1999. G. Strang and T. Nguyen, *Wavelets and Filter Banks*, Wellesley-Cambridge, Wellesley, 1996
4. P. Nunez, et. al., *EEG coherency I: ...*, Electroencephalography & Clin. Neuro. 103: 499-515, 1997
5. J. Bendat and A. Piersol, *Random Data: Analysis and Measurement Procedures*, Wiley-Interscience, New York, 1971. Numerical simulations were performed by the authors.

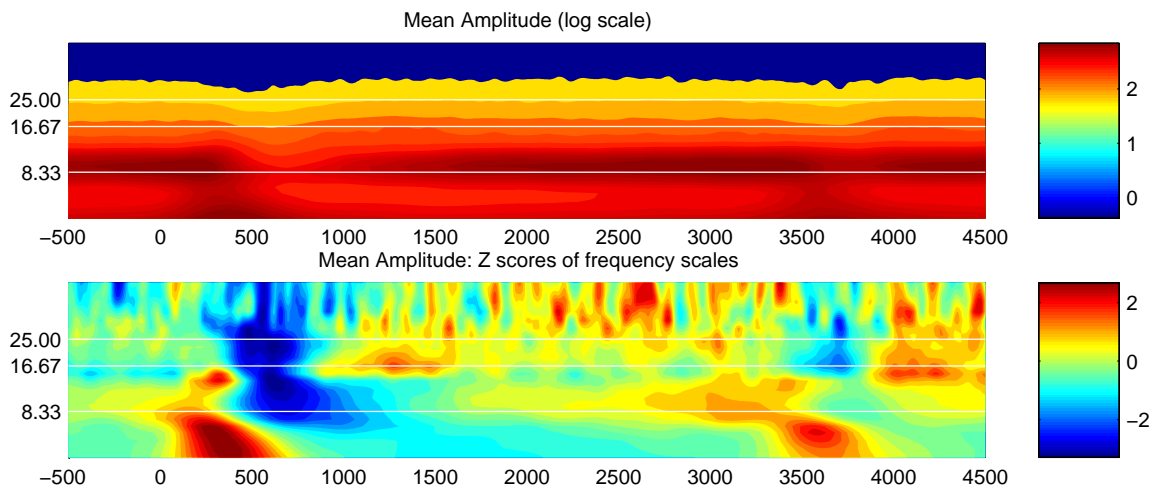


Figure 1. Global Non-Time-Locked Values Averaged across channels and normalized across frequencies

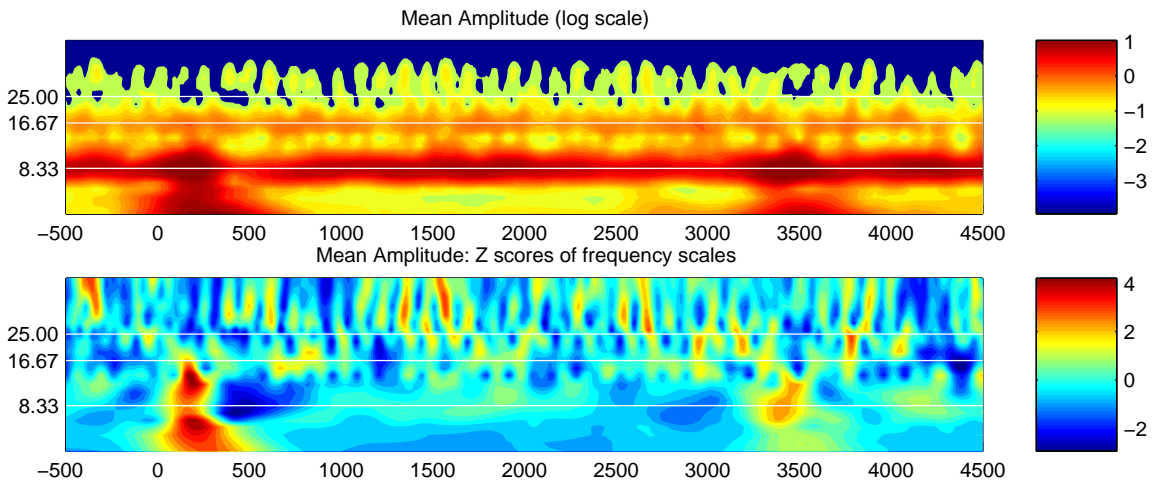


Figure 2. Global Time-Locked Values Averaged across channels and normalized across frequencies

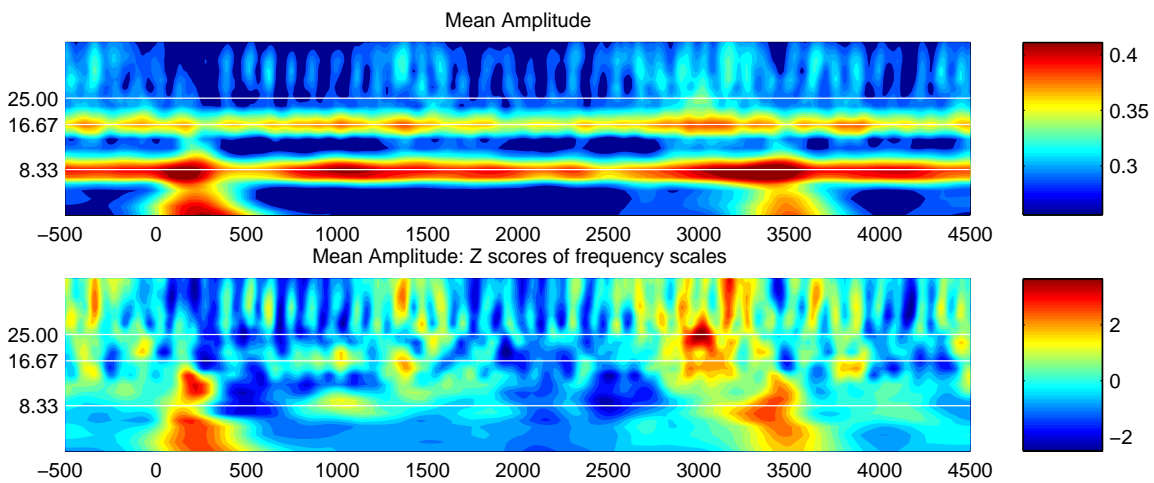


Figure 3. Global ITC Values Averaged across channels and normalized across frequencies

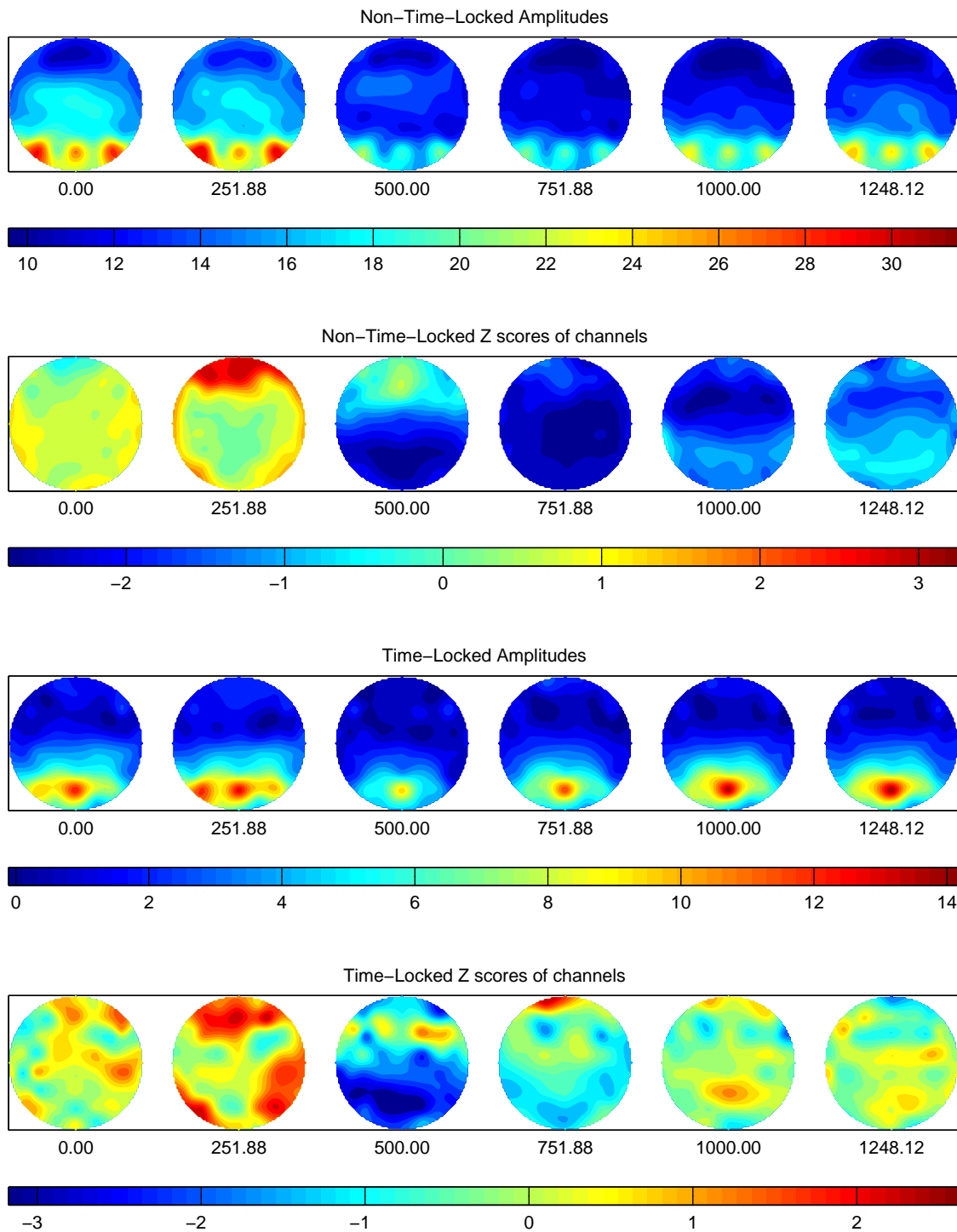


Figure 4: 8 1/3 Hz. Topographic Values. Time in milliseconds from the appearance of the target stimulus beneath the heads. Scale of raw amplitude values or their Z scores shown along colorbars.

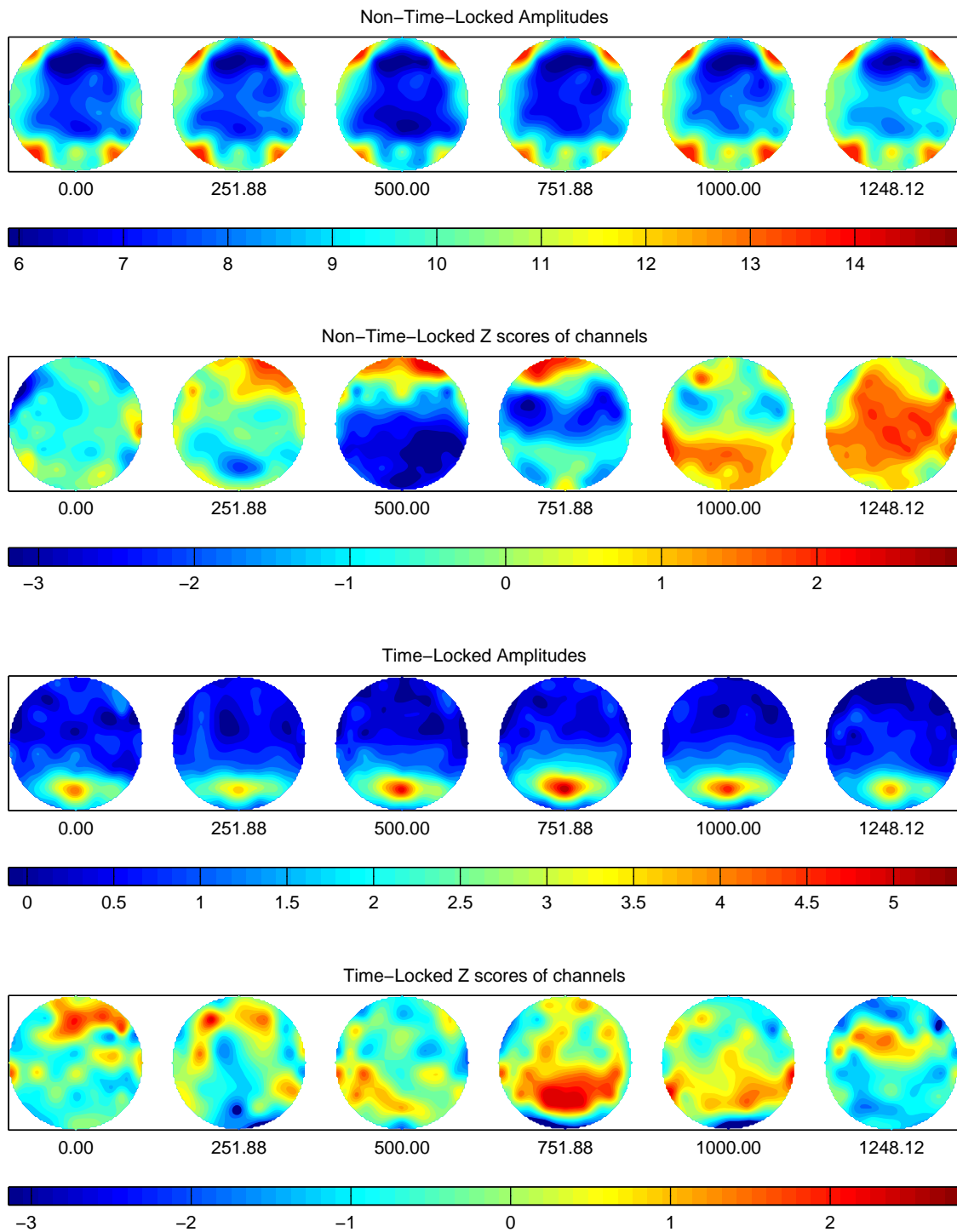


Figure 5. 16 2/3 Hz. Topographic Values Time in milliseconds from the appearance of the target stimulus beneath the heads. Scale of raw amplitude values or their Z scores shown along colorbars.

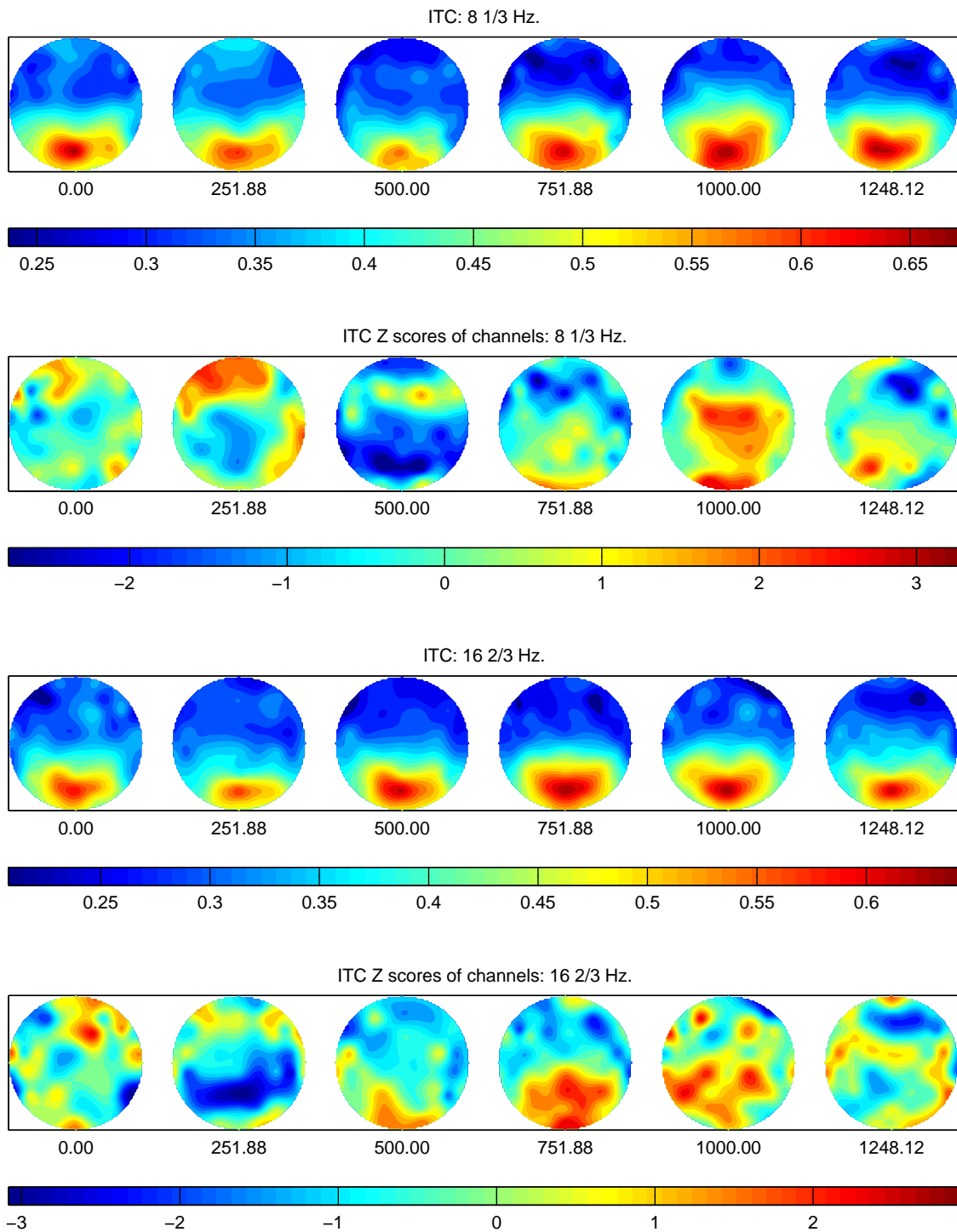


Figure 6. ITC Topographic Values Time in milliseconds from the appearance of the target stimulus beneath the heads. Scale of raw amplitude values or their Z scores shown along colorbars.

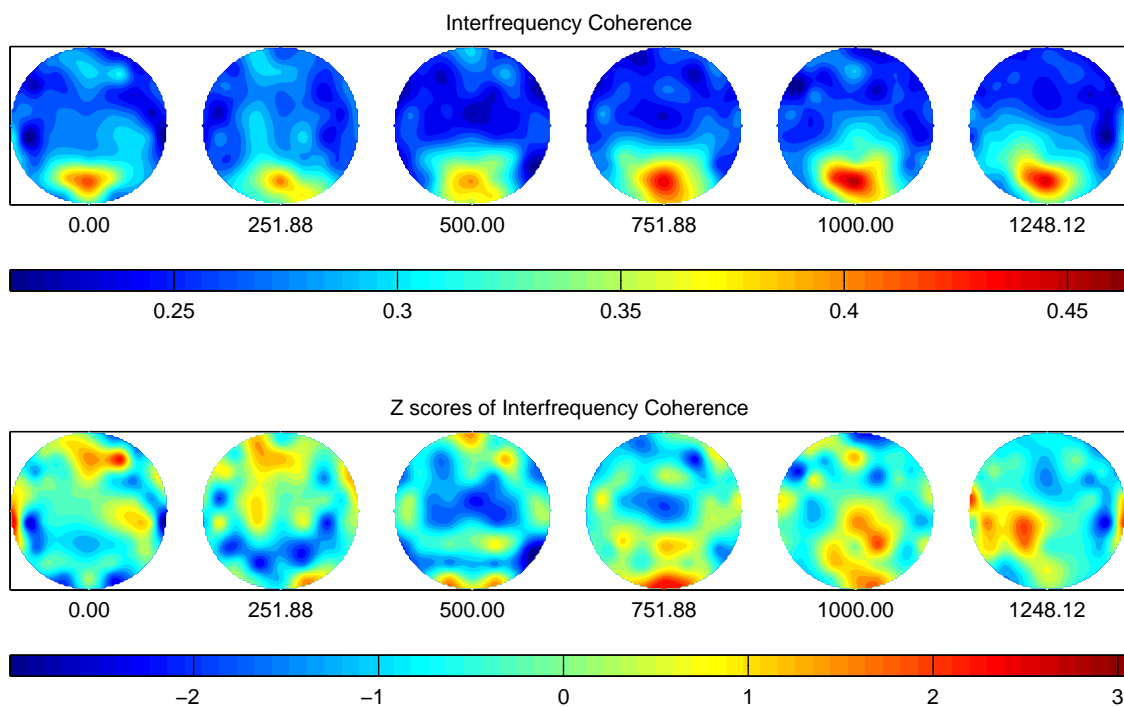


Figure 7. Interfrequency Coherence 8 1/3 Hz. - 16 2/3 Hz. Time in milliseconds from the appearance of the target stimulus beneath the heads. Scale of raw amplitude values or their Z scores shown along colorbars.

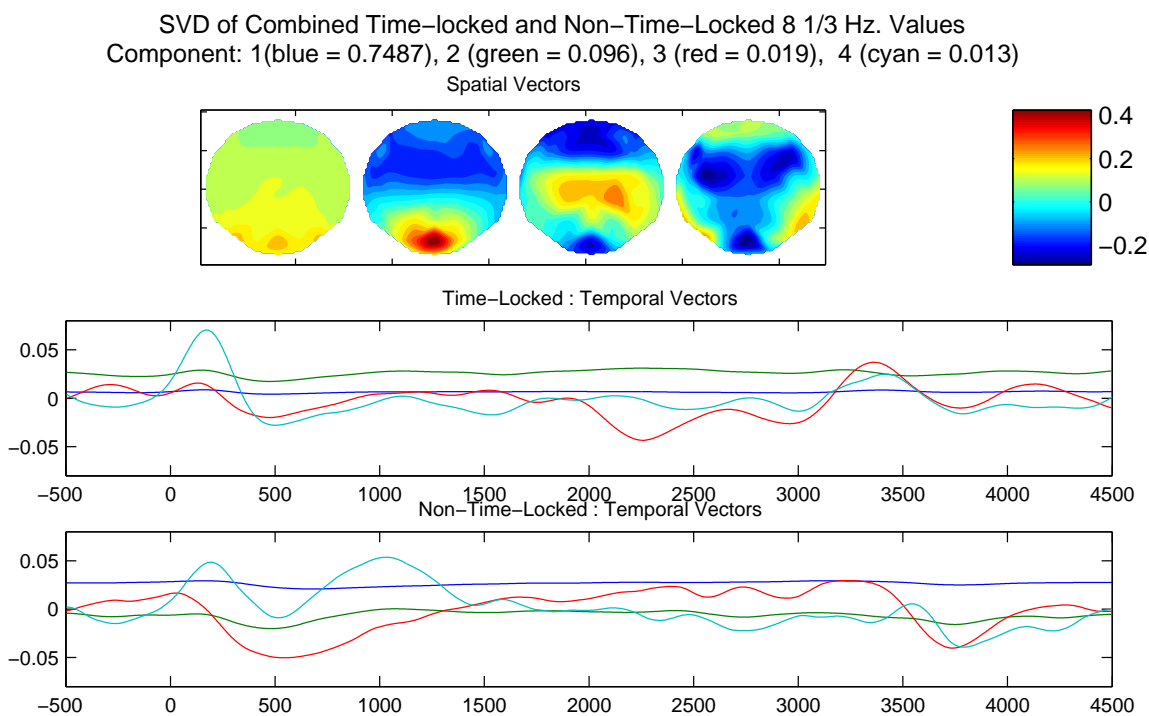


Figure 8. Singular Value Decomposition Spatial and Temporal Components